INVESTIGATION OF THE CIRCULAR MAGNETIZATION
CURVE FOR NICKEL-IRON WIRES UNDER
TORSIONAL AND TENSILE STRESS

by

ARLYN EUGENE ASCH

B. S., Midland College, 1957

———————

A THESIS

submitted in partial fulfillment of the

requirements for the degree

MASTER OF SCIENCE

Department of Physics

KANSAS STATE UNIVERSITY
Manhattan, Kansas

1962

TABLE OF CONTENTS

# INTRODUCTION

As early as 1862 Wiedemann (2) demonstrated that if a longitudinal magnetic field is applied to a circularly magnetized ferromagnetic rod, then besides the longitudinal magnetostriction, the rod twists. This magnetomechanical effect is known as the Wiedemann Effect.

There are two inverses of the Wiedemann Effect:

(1) Twisting a longitudinally magnetized ferromagnetic rod causes circular magnetization of that rod. By reversing the longitudinal field the circular magnetization can be demonstrated by am emf in the direction of the longitudinal field.

(2) Twisting a circularly magnetized ferromagnetic rod causes longitudinal magnetization of that rod. By reversing the circular magnetic field, i.e., the current through the ferromagnetic rod, the longitudinal magnetization can be demonstrated by means of a search coil around the stressed rod.

Since Wiedemann's discovery the inverses of this effect have been "rediscovered" at least twice. First by G. J. van der Maas (11) in 1949 and secondly by W. V. Drumgoole (11) in 1952.

A more general stress-magnetization relationship was first discovered by Joule in 1847 (7). He found that when a ferromagnetic material undergoes magnetization, the physical dimensions of the body change. This is generally referred to as magnetostriction, and is somewhat analogous to electrostriction. A material is said to have a positive linear coefficient of magnetostriction when its length increases in the direction of the applied field upon magnetization and a negative linear coefficient of magnetostriction when it contracts in the direction of the applied magnetic field.

More recently Sixtus and Tonks (9), Dijkstra and Snoek (6), Stewart (10), and others, have investigated the flux reversals in wires under tension. Their work has been primarily concerned with the speed of flux reversal as a function of the tension and the applied field.

The circular and longitudinal magnetization of nickel-iron wires under tensile and torsional stress has been measured by G. J. van der Maas (11). In this work the search coil-ballistic galvanometer method was used to measure the longitudinal magnetization, and the First Inverse Wiedemann effect was utilized to measure the circular magnetization. Under the action of a periodic alternating longitudinal magnetic field the wire changed its magnetization periodically.

For wires under external stress the major portion of this change took place discontinuously at some distinct value of the applied field. Both components of the magnetization vector were measured as functions of the field strength and the applied torsional and tensile stresses. The experimental results obtained indicated that in the region $2 \lesssim H \lesssim 8$ oersteds, the circular and longitudinal components of magnetization increased with torsional stress. It was also shown that these results were independent of the waveform of the applied magnetic field over the range of audio frequencies.

Theoretical investigation of this problem under the assumptions that (a) the magnetocrystalline anisotropy energy is constant or small in comparison with the magnetoelastic and field energies, (b) the change in magnetization takes place quasistatically, and (c) the internal stress is negligible, indicate that with increased twist the circular component of magnetization should increase and the longitudinal component should decrease for all positive values of longitudinal stress, provided that the wire has a positive linear magnetostriction coefficient. Investigations reported in this thesis indicate that for fields above 3 oersteds and twists above 4 deg/cm, increasing twist results in increasing circular magnetization.

It is the purpose of this research to study the magnetomechanical processes in twisted ferromagnetic wires in the reversible region of magnetization $H \gtrsim 0$. Thus the complications which arise from the discontinuous changes in magnetization, characteristic of the irreversible region $-\infty \lesssim H \lesssim +\infty$, are avoided. This thesis will primarily describe attempts to verify experimentally the theoretical expression derived by G. J. van der Maas for the circular magnetization curves of Ni - Fe rods under torsional and tensile stress using the First Inverse Wiedemann effect for the measurement of the circular component of magnetization.

In the First Inverse Wiedemann effect three independent components are closely interrelated, namely, the twist of the wire, the circular magnetic field and the longitudinal magnetic field. Consider a thin-walled twisted cylinder of ferromagnetic material. (See Figure 1) With the application of a longitudinal magnetic field the saturation magnetization vector $I_s$ will align itself along helical paths around the axis of the wire. Thus there will result a circular and a longitudinal component of the magnetization vector.

These components are designated by $I_c$ and $I_l$ respectively. If now any point in the wire is considered, the saturation magnetization vector $I_s$ at that point is found to lie in the plane between the direction of principal stress $\sigma$ and the direction of the applied field H. (See Figure 2) For H = 0, $I_s$ will align itself along the line of principal stress: for H = $\infty$, $I_s$ will align itself in the direction of the applied field. If the applied field is allowed to vary, the direction of the saturation magnetization vector $I_s$ will also vary. This variation of $I_s$ and thereby $I_c$ will produce an electric field directed along the axis of the wire. It is possible to measure the change in circular magnetization by measuring the emf developed in the wire. In this paper a rectified DC current through a coil surrounding the stressed wire was used to produce the needed changing longitudinal magnetic field. By using a rectified DC field the magnetization vector $I_s$ was never allowed to reverse direction, but only "wiggle" toward and away from the line of principal stress.

This work is complementary to work done by G. J. van der Maas and D. D. Bornemeier. D. D. Bornemeier (4) has carried out complementary investigations on the longitudinal component of magnetization.
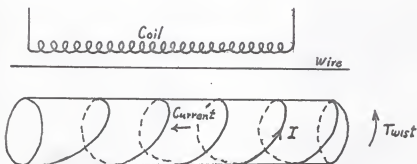


Figure 1.



Figure 2.

# THEORY

## Theory of Magnetization

Domain Theory. In 1907 Weiss (13) explained ferromagnetism in terms of magnetic dipoles, by postulating the existence of a molecular field, which tends to align the individual magnetic dipoles in one direction. Their combined effect thus explained the high field strength associated with magnetized ferromagnetic media. The principle may be seen from the simple couple on a magnetic dipole in a uniform magnetic field. Weiss recognized that the classical magnetic interaction between electrons was much too weak to account for the large magnetic induction values produced by relatively small applied magnetic fields. It is now known that the origin of this field lies in the quantum mechanical exchange forces between electrons. The Weiss molecular field enables saturation magnetization to be obtained spontaneously. In order to permit the possibility of zero magnetization of a material with a zero applied field, Weiss assumed small regions called "domains" within which the local magnetization is at saturation due to the local molecular field. Random orientation of these domains produces zero total magnetization. In general, the volume of these domains varies from $10^{-6}$ cc to $10^{-2}$ cc.

Becker (2) suggested that the increase in magnetization under the influence of an applied field may occur in two independent ways: (a) The growth of favorably oriented domains at the expense of unfavorably oriented domains. (b) Rotation of the entire domain. The first process is characteristic of weak applied fields and the second of stronger applied fields for an unmagnetized sample.

The theoretical explanation of the origin of domains in terms of magnetic field energy was given by Landau and Lifshitz (8). Bitter (3) was first to show the physical existence of domains. Williams, Bozorth and Schockley (14) have shown that the domain shapes and sizes in several ferromagnetic materials under mechanical stress are in good agreement with theory.

The Total Free Energy Expression. Due to the physical shape of the ferromagnetic material used and the range of the applied field, it was possible to neglect two of the terms in the total free energy expression, namely, the exchange energy and the magnetic self energy.

Thus the total free energy $E_t$ at any point in the magnetic material may be expressed as

$$E_t = E_h + E_\sigma + E_k \tag{1}$$

where $E_h$ is the field energy, $E_\sigma$ is the magnetostrictive strain energy or the magnetoelastic energy and $E_k$ is the magnetocrystalline anisotropy energy. The saturation magnetization vector $I_s$ of each domain in the material may be related to a definite direction in the material for each of the energy terms in eqn. (1). For $E_h$ the direction is that of the applied field; for $E_\sigma$ the direction is one of the lines of principal stress and for $E_k$ the direction is one of the crystalographic axes of the crystal. In order to preserve the multivalued property of the relationship between the circular magnetization $I_c$ and the applied field H, the total energy may be expressed in terms of an angular parameter $\Theta$. If $E_t$ is then minimized, the resulting expression is an equation relating I, H and $\Theta$. The component of the saturation magnetization $I_s$ in a direction $\Theta$ from H is related to $I_s$ and $\Theta$ through the relation

$$I_c = I_s \sin \Theta \tag{2}$$

Hence two parametric equations

and

$$\begin{aligned} I_c &= I_c (\Theta) \\ H &= H (\Theta) \end{aligned} \tag{3}$$

represent the circular magnetization curve. It has been pointed out by G. J. van der Maas (12) that minimization of either the total energy or the energy density yield the same relation between $I_c$ and H.

### Significant Terms in the Free Energy Expression

The Field Energy. In order to consider the mutual energy between the magnetization vector and the applied field, consider a domain magnetizated to saturation in a uniform magnetic field. Let $I_s$ designate the saturation magnetization vector of this domain. Then if $I_s$ is initially in the direction of the applied field, the energy required to rotate the domain through an angle $\Theta$ with respect to the external field H is

$$\begin{aligned} E_h &= \int_{\phi=0}^{\Theta} I_s H \sin \Theta \, d\Theta \\ &= I_s H \cos \Theta + I_s H \end{aligned} \tag{4}$$

The Magnetoelastic Energy. The magnetostrictive strain energy or the magnetoelastic energy is closely related to the magnetostriction and its derivation requires a knowledge of the relation between the magnetostrictive change in length of the ferromagnetic material and the stress to which the material is subjected. Becker and Doering (2) have derived this relation for a material having isotropic magnetostriction and no volume magnetostriction, i.e., no change in volume upon magnetization. The result of their computation is given by

$$E_\sigma = \frac{3}{2} \lambda_s \sigma \sin^2\phi - \sigma \lambda_s \qquad (5)$$

where $\lambda_s$ is the saturation magnetostriction constant, $\sigma$ is the stress to which the domain is subjected and $\phi$ is the angle between the saturation magnetization vector $I_s$ and the direction of principal stress. For $\lambda_s > 0$ and $\sigma > 0$, the energy is a minimum for $\phi = 0$, i.e., the application of a positive stress to the rod caused the domains of the wire to become oriented parallel to the line of principal stress. For $\lambda_s < 0$ and $\sigma > 0$, the energy is minimum for $\phi = /2$, i.e., the application of a positive stress to the rod caused the domains of the wire to become oriented perpendicular to the line of principal stress.

For the Ni-Fe wires used in this research $\lambda_s$ was positive for the range of field values used.

The Magnetocrystalline Anisotropy Energy. Experimentally it has been found (5) that magnetization of Ni and Fe crystals is more easily accomplished when the magnetic field is parallel to one of the crystalographic axes of the crystal. When the magnetic field is applied along one of the crystalographic axes, the magnetization vector and the applied field are parallel and one can represent the magnetization as a function of the field strength by magnetization curves. Experimental curves measured for single crystals of nickel and iron (5) with very small amounts of impurities and internal stress (hence small coercive forces and hysteresis effects) indicate that there exist preferred directions of magnetization in the unmagnetized unstressed crystal.

In 1929 Akulov (1) postulated the form of the crystalline anisotropy energy term $E_k$ to be

$$E_k = K_o + K_1(a_1^2 a_2^2 + a_2^2 a_3^2 + a_3^2 a_1^2) + K_2(a_1^2 a_2^2 a_3^2) + \text{higher order terms} \qquad (6)$$

where the a's are the direction cosines of the magnetization vector in the crystal with respect to the crystallographic axes and the K's are the anisotropy constants characteristic of the material.

For polycrystalline materials this energy term is negligible if the crystals are randomly oriented. Application of a moderate amount of longitudinal stress will reduce the effect of the magnetocrystalline anisotropy energy in comparison with the other energy terms in the free energy expression.

## The Circular Magnetization Curve

The theory which follows assumes the minimum energy principle, i.e., the magnitude and direction of the magnetization vector will be such that the total free energy is minimum, and is strictly valid only for reversible rotations of the domains, i.e., in the reversible region $H \gtrsim 0$.

Minimization of the Free Energy Expression. A stress analysis of the wire shows that there exist only two directions of principal stress at any point in a wire under pure torsion, one tensile and the other compressive. In the appendix a determination of the directions and magnitudes of principle stress are given in detail. It is shown that the directions of principal stress in the rod are perpendicular to the radius vector (which is perpendicular to the axis of the twisted wire) and each make an angle of $45^\circ$ with the axis of the wire. It can also be shown (12) that the application of a longitudinal stress to the wire serves only to reduce the angle between the line of principal stress and the axis of the wire.

It is also assumed that the internal stress in the wire is negligible and that the magnetoelastic energy term $E_k$ in equation (1) is negligibly small, i.e., there is very little texture to the wire.

Since the Ni-Fe wires used in this research had a positive linear saturation magnetostriction constant, the action of the compressive stress $\sigma$ with respect to the magnetoelastic energy term $E_\sigma$ is equivalent to a perpendicular stress of equal magnitude. Thus equation (5) becomes

$$E_\sigma = 3 \lambda_s \sigma_+ \sin^2\emptyset + \text{const.}$$

where $\sigma_+$ is the tensile stress. The expression for the total free energy is then

$$E_t = - I_s H \cos \Theta + I_s H + 3 \lambda_s \sigma_+ \sin^2\emptyset + \text{const.} \tag{7}$$

Consider a ferromagnetic rod with one end fixed. Under twist the direction of principal tensile stress will be perpendicular to the radius vector and make an angle of $45^\circ$ with the axis of the rod.

Figure 3 represents the position of the saturation magnetization vector at some point in the rod at a distance $\rho$ from the axis.
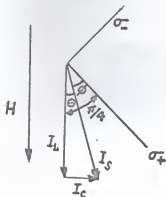


Figure 3

Since H, $I_s$ and $\sigma_+$ are coplanar, $\emptyset = 45^0 - \Theta$. Using this relation in equation (7) gives

$$E_t = - I_s H \cos \Theta + 3 \lambda_s \sigma_+ \sin^2 (45^0 - \Theta) + \text{const.} \qquad (8)$$

The conditions which ensure that the total free energy will be minimum are

$$dE_t/d\Theta = 0 \qquad (9)$$

and

$$d^2E_t/d\Theta^2 > 0 \qquad (10)$$

Applying the first minimal condition to equation (8) gives

$$I_s H \sin \Theta - 3 \lambda_s \sigma_+ \cos 2\Theta = 0 \qquad (11)$$

Applying the second minimal condition to equation (8) gives

$$I_s H \cos \Theta + 6 \lambda_s \sigma_+ \sin 2\Theta > 0 \qquad (12)$$

Since $I_s$, H, $\lambda_s$ and $\sigma_+$ are all positive, it is seen that there are two minimal positions for the magnetization vector. These two positions are illustrated in Figure 4.
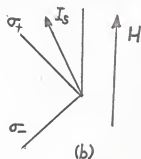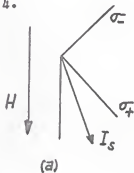


(a)

Figure 4

(b)

Figure 4a shows the case for a downwardly applied magnetic field, while Figure 4b shows the case for an upwardly applied magnetic field. If the magnetic field is reversed, the $I_s$ vector will be in an unstable position and at a particular value of the applied field (called the "jump-field"), the $I_s$ vector will "flip" to a stable position in the opposite direction.

In either case the value of the circular component of magnetization $I_c$ is given by

$$I_c = I_s \sin \theta \qquad (13)$$

Any change in the position of the saturation magnetization vector $I_s$ will cause a change in the circular component of the magnetization vector $I_c$ and this change of circular flux will induce an electric field directed along the wire.

The circular magnetization process may be qualitatively described as follows: As the amount of twist applied to the wire is increased, the magnitude of the principal stress will increase. In order that equation (11) remain valid, $\theta$ must increase or $I_s$ must assume a position closer to the line of principal stress. As the magnitude of the applied field is increased, the position $I_s$ will assume according to equation (11) is one such that $\theta$ will decrease.

Application of a rectified DC longitudinal magnetic field along the axis of a rod initially magnetized in a direction parallel to this field can never cause the $I_s$ vector to reverse direction or "flip"; at most the $I_s$ vector can only oscillate between the direction of principal stress and the direction of the applied field in a manner such that equation (11) remains valid.

The Voltage Developed at the Ends of the Wire. Since the circular component of magnetization $I_c$ is continually changing magnitude, the circular flux around the wire is also changing. From Faraday's Law it is seen this changing flux will generate an emf between the ends of the wire. To determine the relation between the voltage developed at the ends of the wire and the circular flux, consider a twisted elemental cylinder of the wire at a distance $\rho$ from the center of the rod of thickness $d\rho$ and length $\ell$. Refer to Figure 5.
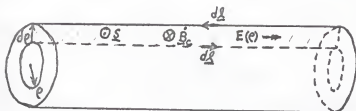


Figure 5

The electric field $E(\rho)$ may be related to the circular component of the flux through one of Maxwell equations, namely

$$\nabla \times \underline{E} = -\frac{dB}{dt}c$$

or

$$\oint \underline{E}(\rho) \cdot d\underline{\ell} = -\iint_S \underline{\dot{B}}_c \cdot d\underline{S}$$

where $\underline{S} = \underline{\ell}\, d\rho$ and is a direction antiparallel to $\underline{\dot{B}}_c$  The line integral is taken around the area $\underline{S}$.  Integration yields

$$\ell\left[E(\rho) - E(r)\right] = -\ell \int_\rho^r \dot{B}_c \cos\pi\, d\rho = \ell \int_\rho^r \dot{B}_c\, d\rho$$

$$= -\ell \int_r^\rho \dot{B}_c\, d\rho \tag{14}$$

Since $E(r) = 0$, equation (14) becomes

$$E(\rho) = -\int_r^\rho \dot{B}_c\, d\rho \tag{15}$$

Taking the partial derivative of equation (15) with respect to  gives

$$\frac{\partial E(\rho)}{\partial \rho} = -\dot{B}_c \tag{16}$$

The voltage $V_m$ measured at the ends of the wire is, be definition

$$V_m = -\overline{E}\,\ell \tag{17}$$

where $\overline{E}$ is the effective electric field over the cross section of the wire. It is shown in the Appendix that

$$\overline{E} = \frac{1}{\pi r^2} \int_0^r E(\rho)\, 2\pi\rho\, d\rho \tag{18}$$

or

$$\overline{E} = \frac{1}{r^2} \int_0^{r^2} E(\rho)\, d\rho^2 \tag{19}$$

Substitution of Equation (19) into equation (17) yields

$$V_m = - \frac{\ell}{r^2} \int_o^{r^2} E(\rho) \, d\rho^2$$

Integration by parts gives

$$V_m = - \frac{\ell}{r^2} \left[ E(\rho) \, \rho^2 \Big|_o^{r^2} - \int_{\rho=o}^{\rho=r} \rho^2 \, d\left(E(\rho)\right) \right]$$

$$= \frac{\ell}{r^2} \int_o^{\rho} \frac{\partial E(\rho)}{\partial \rho} \rho^2 \, d\rho$$

Substitution of equation (16) into the above relation gives

$$V_m = - \frac{\ell}{r^2} \int_o^r \dot{B}_c \, \rho^2 \, d\rho$$

Integration the above relation over time gives

$$\int V_m dt = - \frac{\ell}{r^2} \int_o^t dt \int_o^r \dot{B}_c \, \rho^2 \, d\rho \tag{20}$$

$$= - \frac{\ell}{r^2} \int_o^r B_c \, \rho^2 \, d\rho$$

Since $V_m dt$ has the dimensions of flux, the following designation is made.

$$\int V_m dt \equiv \overline{\Delta\emptyset}$$

where $\overline{\Delta\emptyset}$ is the effective change in circular flux over the cross sectional area of the wire.

The total flux $\Delta\emptyset \, (\rho)$ encircling that portion of the wire of radius $\rho$ is given by

$$\Delta\emptyset(\rho) = \iint_S \underline{B}_c \cdot d\underline{S}$$

or $\tag{21}$

$$= \ell \int_\rho^r B_c \, d\rho$$

Taking the partial derivative of equation (21) with respect to $\rho$ yields

$$\frac{\partial \, \Delta\varnothing(\rho)}{\partial \rho} = \ell \, B_c \qquad (22)$$

Substitution of equation (22) into equation (20) gives

$$\overline{\Delta\varnothing} = -\frac{1}{r^2} \int_0^r \frac{\partial \Delta\varnothing(\rho)}{\partial \rho} \, \rho^2 \, d\rho$$

$$= -\frac{1}{r^2} \int_{\rho=0}^{\rho=r} \rho^2 \, d\left(\Delta\varnothing(\rho)\right)$$

Integration by parts yields

$$\overline{\Delta\varnothing} = -\frac{1}{r^2} \left[ \rho^2 \Delta\varnothing(\rho) \Big|_0^r - \int_0^{r^2} \Delta\varnothing(\rho) \, d\rho^2 \right]$$

Noting that $\Delta\varnothing(\rho)\big|_{\rho \, = \, r} = 0$ gives

$$\overline{\Delta\varnothing} = \frac{1}{r^2} \int_0^{r^2} \Delta\varnothing(\rho) \, d\rho^2 \qquad (23)$$

Since the voltage time integral is a measure of the average flux change over the cross sectional area of the wire, it is now possible to derive a set of parametric equations which represent the circular magnetization curve.

Parametric Equations Relating $\overline{\Delta\varnothing}$ and $\underline{H}$. It is noted that   and $\Theta$ are not independent variables, but are connected through the equations

$$\sigma_+ = G \frac{d\phi}{dl} \rho \qquad (24)$$

$$HI_s \sin\Theta = 3 \, \lambda_s \, \sigma_+ \cos 2\Theta \qquad (11)$$

Equation (24) is derived in the Appendix. Solving for $\rho$ and substituting equation (24) into equation (11) gives

$$\rho = \frac{I_s \, H}{3 \, \lambda_s \, G \, \frac{d\phi}{d\ell}} \, \frac{\sin\Theta}{\cos 2\Theta} \qquad (25)$$

$$d\rho = \frac{I_s \, H}{3 \, \lambda_s \, G \, \frac{d\phi}{d\ell}} \, d\left(\frac{\sin\Theta}{\cos 2\Theta}\right) \qquad (26)$$

$$d\rho^2 = \left[\frac{I_s \, H}{3 \, \lambda_s \, G \, \frac{d\phi}{d\ell}}\right]^2 d\left(\frac{\sin^2\Theta}{\cos^2 2\Theta}\right) \qquad (27)$$

Substituting equation (26) into equation (21) and using the fact that $B_c$ = $I_c$ = $I_s \sin \Theta$ yields

$$\Delta\emptyset(\rho) = \frac{\ell \, I_s^2 \, H}{3 \, \lambda_s \, G \, \frac{d\emptyset}{d\ell}} \int_{\rho=\rho}^{\rho=r} \sin\Theta \; d\left(\frac{\sin\Theta}{\cos 2\Theta}\right) \tag{28a}$$

Integration by parts yields

$$\Delta\emptyset(\rho) = \frac{\ell \, I_s^2 \, H}{3 \, \lambda_s \, G \, \frac{d\emptyset}{d\ell}} \left[\frac{\sin^2\Theta}{\cos 2\Theta} + \frac{1}{4} \ell n \, |\cos 2\Theta|\right]_{\Theta_\rho}^{\Theta_r} \tag{28b}$$

The details of the above integration are shown in the Appendix. Substitution of equation (28b) into equation (23) yields

$$\overline{\Delta\emptyset} = \frac{\ell \, I_s^2 \, H}{3 \, \lambda_s \, G \, \frac{d\emptyset}{d\ell}} \int_0^r \left[\frac{\sin^2\Theta}{\cos 2\Theta} + \frac{1}{4} \ell n \, |\cos 2\Theta|\right]_{\Theta_\rho}^{\Theta_r} d\rho^2$$

Using equation (27) in the above relation gives

$$\overline{\Delta\emptyset} = \frac{\ell \, I_s}{r^2} \left[\frac{I_s \, H}{3 \, \lambda_s \, G \, \frac{d\emptyset}{d\ell}}\right]^3 \int_{\rho=0}^{\rho=r} \left[\frac{\sin^2\Theta}{\cos 2\Theta} + \frac{1}{4} \ell n \, |\cos 2\Theta|\right]_{\Theta_\rho}^{\Theta_r} d\left(\frac{\sin^4\Theta_\rho}{\cos^2 2\Theta_\rho}\right) \tag{29a}$$

Integration yields

$$\overline{\Delta\emptyset} = \frac{\ell \, I_s \, r}{\sin^3\Theta_r} \left[\frac{1}{12} - \frac{3}{16} \cos 2\Theta_r + \frac{1}{8} \cos^2 2\Theta_r - \frac{1}{48} \cos^3 2\Theta_r\right] \tag{29b}$$

The details of the above integration are shown in the Appendix.

The equation for the magnetic field may be found from equations (24) and (11)

$$H = \frac{3 \lambda_s \, G \, r \, \frac{d\emptyset}{d\ell}}{I_s} \; \frac{\cos 2\Theta_r}{\sin\Theta_r} \tag{30}$$

Equation (29b) and (30) are the parametric expression for the total circular flux as a function of the applied field. The subscript r may be dropped in that $\Theta_r$ is only a parameter. Hence

$$\overline{\Delta\emptyset} = \frac{\ell \, I_s \, r}{\sin^3\Theta} \left[\frac{1}{12} - \frac{3}{16} \cos 2\Theta + \frac{1}{8} \cos^2 2\Theta - \frac{1}{48} \cos^3 2\Theta\right]$$

$$H = \frac{3 \lambda_s \, G \, r \, \frac{d\emptyset}{d\ell}}{I_s} \; \frac{\cos 2\Theta}{\sin\Theta} \tag{31}$$

Plate I is a plot of the circular magnetization curve using the equations given above for values of the parameter $\Theta$ ranging from 0 to $45^\circ$. This theoretical curve is in qualitative agreement with the phenomenological picture. One should find $\overline{\Delta\emptyset} = 0$ for H infinitely large and $\overline{\Delta\emptyset}$ maximum for H = 0.
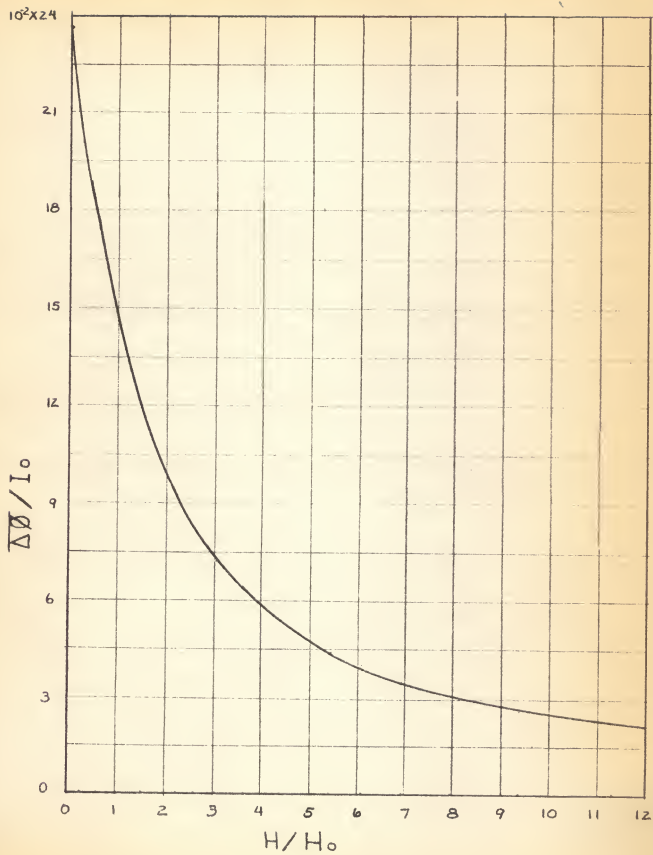
The Theoretical Circular Magnetization Curve.

This curve was made using equation (31) for values of the parameter $\theta$ ranging from 0 to $45^\circ$, where

$$I_o = 1\ I_s r$$

$$H_o = \frac{3\lambda\ Gr}{I_s}\ \frac{d\phi}{dl}$$

It is noted that this plot is dimensionless and independent of the magnitude of the twist.

# PLATE I

The experimental measurement of the time integral of the voltage pulse developed at the ends of the wire gave $\overline{\Delta\phi}_{max} - \overline{\Delta\phi}$ not $\overline{\Delta\phi}$. This quantity was designated by $d\overline{\Delta\phi}$. In order to compare the experimentally measured values with the theoretically predicted values, a second theoretical curve plotting $d\overline{\Delta\phi}$ versus H was made. This curve is shown in Plate II.

Plate III is a plot of the change in the circular component of magnetization $d\overline{\Delta\phi}$ versus the applied field H for values of the parameter $\theta$ ranging from 0 to $45^{\circ}$ with $G = 5.87 \times 10^{11}$ dyne/cm$^2$, $\lambda_s = 23.9 \times 10^{-6}$, $I_s = 1.6 \times 10^{4}/4$ u.p./cm$^2$, $r = 1.265 \times 10^{-2}$ cm, $l = 80.0$ cm and $d\phi/dl$ in multiples of $2\pi/110$ rad/cm. One turn (1 T) was equivalent to a twist of 3.28 deg/cm.

It is also noted that if the parameter $\theta$ is eliminated between the equations in (31), $\overline{\Delta\phi}$ or $d\overline{\Delta\phi}$ is a function of $\frac{H}{d\phi/dl}$ alone. The functional dependence of $d\overline{\Delta\phi}$ on $\frac{H}{d\phi/dl}$ was also checked in this work.

EXPLANATION OF PLATE II

The theoretical magnetization curve used for experimental comparisons,
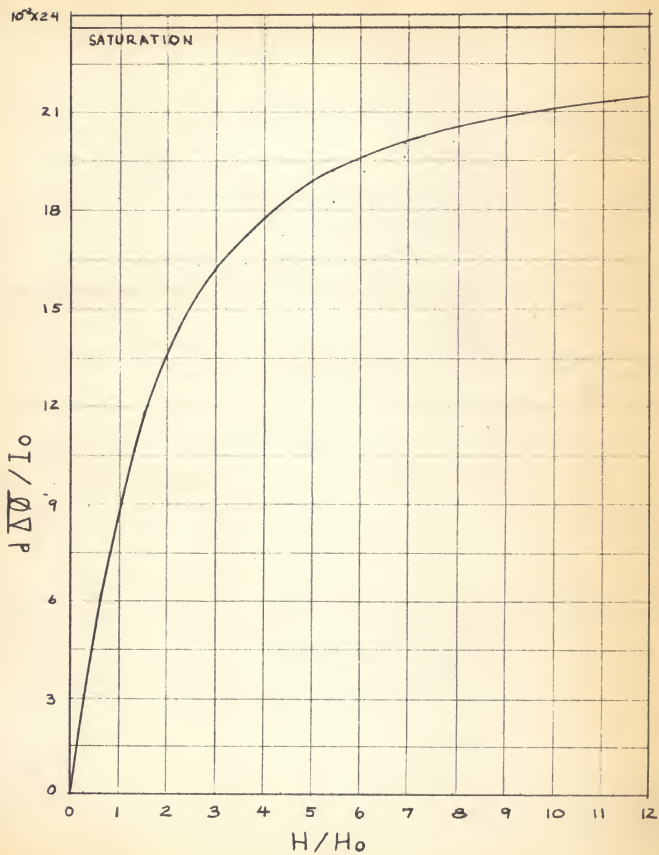i.e., a plot of $\frac{d\Delta\phi}{I_o}$ versus $H/H_o$ where

$$I_o = lI_s r$$

and

$$H_o = \frac{3\lambda_s G}{I_s} \frac{d\phi}{dl}$$

It is noted that this plot is dimensionless and independent of the magnitude
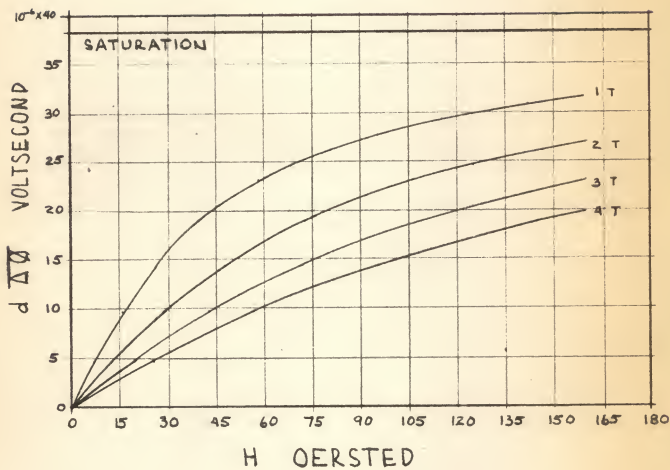of the twist.

# PLATE II

# PLATE Ⅲ

## EXPERIMENTAL METHOD

### General Principle

For measurement of the circular component of magnetization, the wire sample was placed in a field coil which produced the necessary longitudinal magnetic field. The magnetization of the sample was changed by variation of the magnitude of the current in the field coil. The voltage pulse developed at the ends of the sample was picked up across a resistor in parallel with the ends of the wire, electrically integrated and $d\overline{\Delta\phi}$ was read directly by an oscilloscope.

The magnetic field inside the field coil is given by

$$H = \frac{4\pi Ni}{10}$$

where N is the turns/cm on the field coil, i is the current in amperes through the field coil, and H is measured in oersteds. A calculation of the demagnetizing fields due to the finite length of the coil and the presents of the wire showed these fields could be neglected.

### Basic Apparatus

The basic apparatus (refer to Plate IV) consisted of two identical vertically mounted field coils, K and L, 89.5 cm in length with a mean diameter of 1.05 cm. Each field coil contained 1040 turns of copper wire. The second coil L was not used in the measurement of the circular component of magnetization. The Ni-Fe wire sample G was placed inside the field coil K. The top of the wire was held by a chuck F which could be rotated by the adjustment knob A in either direction through any desired angle. The magnitude of this angular displacement was measured by a $360^{\circ}$ scale, B, and the pointer C. The lower end of the wire sample was attached to a weight holder V. An adjustable plexi-glass tab holder U was positioned below the field coil. This holder in conjunction with a small rectangular piece metal T welded or glued to the sample prevented the bottom end of the wire from turning when torque was applied. The voltage, which was generated at the ends of the sample, was picked up through mercury contacts H and S placed inside the field coil. These contacts provided good electrical contact with the sample without hampering the movement of the wire when torque was applied. A cross section of the lower contact W reveals that the sample as well as a platinum lead R were surrounded by a pool of mercury Q.

The pool of mercury was located approximately 5 cm from the end of the field coil. The capsule P which held the mercury and the platinum lead was machined from a fiber rod. The platinum lead was soldered to a small diameter copper lead just below the fiber capsule and this lead was attached to the binding posts at O. Two 5000 turn search coils I and J were used for measurement of the change in the longitudinal component of magnetization. The base of the apparatus was fitted with four leveling screws D. All materials used in the construction of the basis apparatus were non-ferromagnetic: the frame was constructed from 0.635 cm aluminum alloy plate. A polyethylene insulation layer E inserted between the chuck and the frame together with the plexi-glass holder U made it possible to hold the sample at any desired potential. In order to facilitate the connection of the basis apparatus to auxiliary equipment, binding posts M, N and O were placed on the side of the apparatus.

Plate V is a schematic of the experimental arrangement used.

## The RC Integrator

An RC integrator shown in Figure 1, Plate VI was used to electrically integrate the voltage pulse developed at the ends of the torqued wire. This integrator was found to be wave form dependent.

Figure 2, Plate VI shows the input and the output voltages of the integrator. Because the integrator was wave form dependent, the calibration curve of the integrator has been determined experimentally using voltage pulse of a typical wire sample. This curve was found to be nearly linear.

The phase shift between the output wave form of the integrator and that of the applied field was found to be negligible.

## Wire Constants

D. D. Bornemeier (4) carried out measurements determing the necessary constants of the Ni-Fe wires used in this research. These values were used in the calculations of this thesis. The wire used was 51 percent nickel and 49 percent iron.
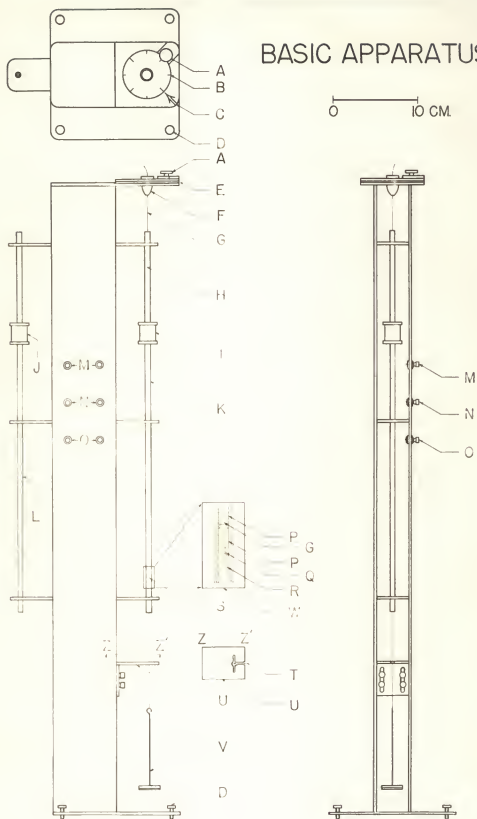
## EXPLANATION OF PLATE IV

### Drawing of Basis Apparatus

| | |
|---|---|
| Adjustment Knob | A |
| $360°$ Scale | B |
| Pointer | C |
| Leveling Screws | D |
| Polyethylene Insulation Layer | E |
| Chuck | F |
| Ni-Fe Wire | G |
| Position of Upper Mercury Contact | H |
| Search Coil | I |
| Search Coil | J |
| Field Coil No. I | K |
| Field Coil No. II | L |
| Search Coil Binding Posts | M |
| Field Coil Binding Posts | N |
| Mercury Contact Binding Posts | O |
| Cap and Body of Fiber Contact | P |
| Mercury Pool | Q |
| Platinum Wire Lead | R |
| Position of Lower Mercury Contact | S |
| Metal Tab Attached to Wire | T |
| Adjustable Plexi-glass Holder | U |
| Weight Holder | V |
| Cross Section of Lower Mercury Contact | W |

PLATE IV



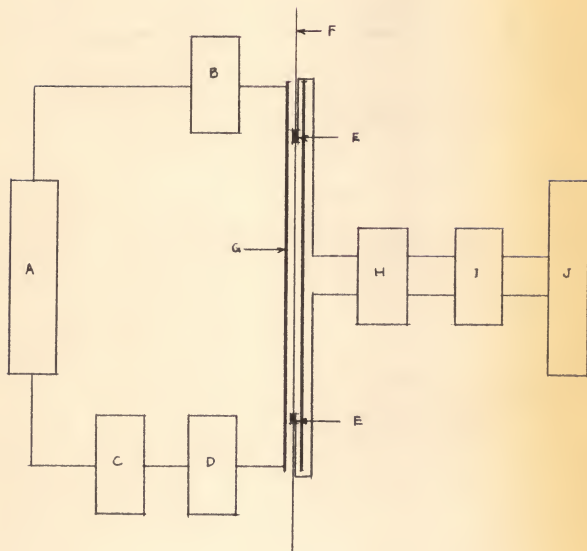BASIC APPARATUS

0 ⊢————⊣ 10 CM.

EXPLANATION OF PLATE V

Schematic of the Experimental Arrangement.

      A.  Variac

      B.  Half-wave rectifier

      C.  Meters

      D.  Variable resistances

      E.  Mercury contacts

      F.  Ni-Fe wire

      G.  Field Coil

      H.  Resistor

      I.  Integrating circuit

      J.  Oscilloscope

# PLATE Ⅴ

EXPLANATION OF PLATE VI

Figure 1.  Schematic of the Integrating Circuit.
Figure 2.  Input and output wave form of the Integrating Circuit.

                    A.  1 1/2 TR
                    B.  2 1/2 TR
                    C.  1 1/2 TL
                    D.  2 1/2 TL
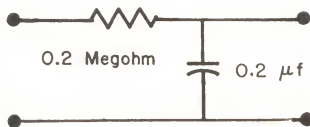                    E.  1     TR

# PLATE VI



Figure 1



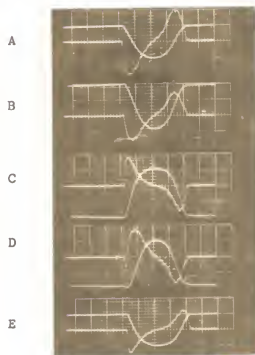Figure 2

## Polarization of the Sample

The Problem. The polarization of a polycrystalline ferromagnetic which
has no texture or internal stress may be accomplished by subjecting the material
to an intense magnetic field. In general, all fabricated metals such as those
used in this work possess a certain degree of internal structure, thus, the remanent
magnetization of this material may vary to great extent. From the theory out-
lined above it is clear that in this work polarization meant magnetization of the
wire so that it formed one macrodomain, i.e., there were no domains of reversed
magnetization in the sample. It was impossible to determine when or if this con-
dition was reached for the samples used in that the internal stresses and texture
were not known.

Preparation of the Sample. In this work a method of annealing has been used
to obtain a higher degree of polarization of the samples. The wire was received
from the manufacturer wrapped on spools approximately 1 1/2 inches in diameter.
When a sample was cut from one of these spools it was found to "coil" readily.
In order to eliminate this undesirable property, the sample was allowed to hang
under a constant tensile stress for a long period of time (2-6 months). When the
sample was placed under a tensile stress, it was heated to a cherry red color by
use of an AC current through the sample and cooled to room temperature. The cooling
was rapid, about two minutes. While ordinary annealing tends to relieve inter-
nal stresses, annealing under tensile stress (as described above) only tends to
reorient the internal stresses. It was also noted that the above described pro-
cess entirely eliminated the tendency of the sample to "coil".

The sample was then carefully placed in the field coil of the apparatus and
magnetically annealed. In this process the sample was heated until its temperature
exceeded its curie point temperature. Again the sample was heated by an AC cur-
rent through the sample. After an equilibrium temperature was reached (approxi-
mately 10 seconds after the current was turned on), the field coil was energized
to produce a longitudinal magnetic field of about 180 oersteds. Then the current
through the sample was cut off, and the sample was allowed to cool rapidly (4-5
seconds) through its curie temperature to room temperature while in a longitudinal
magnetic field and under a constant tensile stress and no torsional stress. When
the wire had reached room temperature the longitudinal field was gradually reduced
to approximately 7 oersteds. Rapid cooling of the sample was objectionable be-
cause of the possibility of introducing large internal stresses.

However, if the annealing current were maintained, the wire would also be sub-
jected to an alternating circular magnetic field, and possibly retain an unwanted
circular component of magnetization.

### RESULTS

Plates VII and VIII display the experimentally obtained relationships be-
tween $d\Delta\overline{\emptyset}$ and $H_c$. It is noted that there exists a curve, contrary to theory, for
$\frac{d\emptyset}{dl} = 0$. This would seem to indicate that the sample still possessed a certain
amount of internal stress equivalent to twisting the wire to the right. Twisting
the wire to the left produced a smaller change in circular flux than twisting the
wire to the right for a given value of the applied field. All samples tested
yielded a set of curves similar to those shown in these Plates.

In Plates IX and X the curve for $\frac{d\emptyset}{dl} = 0$ has been added, according to sign,
to the curves shown in Plates VII and VIII. It is noted that the set of curves
for twisting the wire to the right are mirrored, within ten percent, by the set
of curves for twisting the wire to the left. The curves shown in Plates IX and
X are of the general shape and symmetry predicted by the simple theoretical model
developed in this thesis.

The experimentally found values of $d\Delta\overline{\emptyset}$ are 25 to 30 percent less than the
theoretically predicted values of $d\Delta\emptyset$. A precise quantitative comparison is dif-
ficult since the exact nature of both the internal stress and the texture of
the samples before and after polarization was not known and neither of these factors
were considered in the theoretical model. Since no consideration was made for the
existence of internal stress or texture in wire, and the degree of polarization
of the wire was not known, the percentage difference between the theoretical and
experimental curves is reasonable. Probably the greater share of this difference
was due to ineffective polarization of the wire.

A portion of the experimental error may be attributed to the fact that all
measurements were carried out with approximately $0.1$ kg/mm$^2$ longitudinal tensile
stress on the wire sample. Extrapolation of curves plotting $d\Delta\overline{\emptyset}$ versus the
applied longitudinal stress for different values of the applied field to give
$d\Delta\overline{\emptyset}$ for zero longitudinal stress indicate that the effect of longitudinal stresses
reduced the value of $d\Delta\overline{\emptyset}$.

For the longitudinal stress applied to the samples $d\overline{\Delta\phi}$ was reduced by less than two percent, so no correction was made for this source of error.

Plates XI and XII display the experimentally found relationship between $d\overline{\Delta\phi}$ and $\frac{H}{d\phi/dl}$ for $\frac{d\phi}{dl} = 1, 2, 3$ and $4$ turns. The data for these plates is the same as that used in Plate IX. Plates XI and XII are representative of the samples tested. It is seen that $d\overline{\Delta\phi}$ is nearly a function of $\frac{H}{d\phi/dl}$ alone for $\frac{d\phi}{dl} = 2, 3$ and $4$ turns. For $\frac{d\phi}{dl} = 1$ turn, $d\overline{\Delta\phi}$ is a function of $\frac{H}{d\phi/dl}$ alone for small values of $\frac{H}{d\phi/dl}$. It was found experimentally that the relationship between $d\overline{\Delta\phi}$ and $d\phi/dl$ for the range of values of the applied field used possessed a maximum for $\frac{d\phi}{dl}$ between $3/4$ and $1\,1/4$ turn. Theoretically $d\overline{\Delta\phi}$ should approach a maximum as $\frac{d\phi}{dl}$ approaches zero, but for $\frac{d\phi}{dl} = 0$, $d\overline{\Delta\phi} = 0$. The difference between the theoretically predicted relation and the experimentally found relation may be attributed to the non-ideal properties of the samples used, i.e., the internal stress and the texture of the sample. Since $\frac{d\phi}{dl} = 1$ turn lies in a region where the theory is inadequate, the variations seen in Plates XI and XII are not unreasonable.

EXPLANATION OF PLATE VII

The experimental magnetization curves for different values of angular
displacement (T). One turn equals 3.28 deg/cm. TR designates "turns to
right" and TL designates "turns to the left".
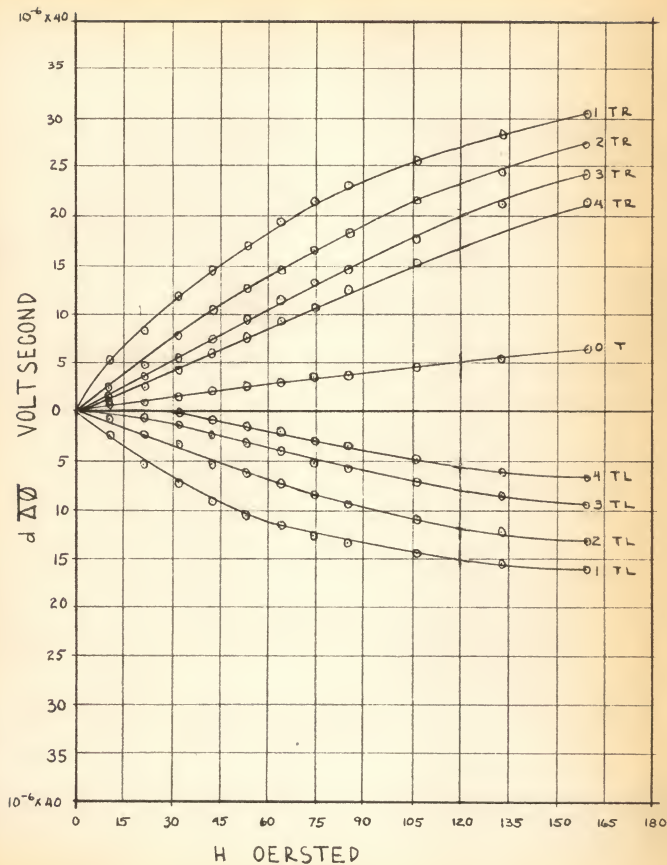
# PLATE VII

EXPLANATION OF PLATE VIII

The experimental magnetization curves for different values of angular displacement (T).  One turn equals 3.28 deg/cm.  TR designates "turns to right" and TL designates "turns to the left."
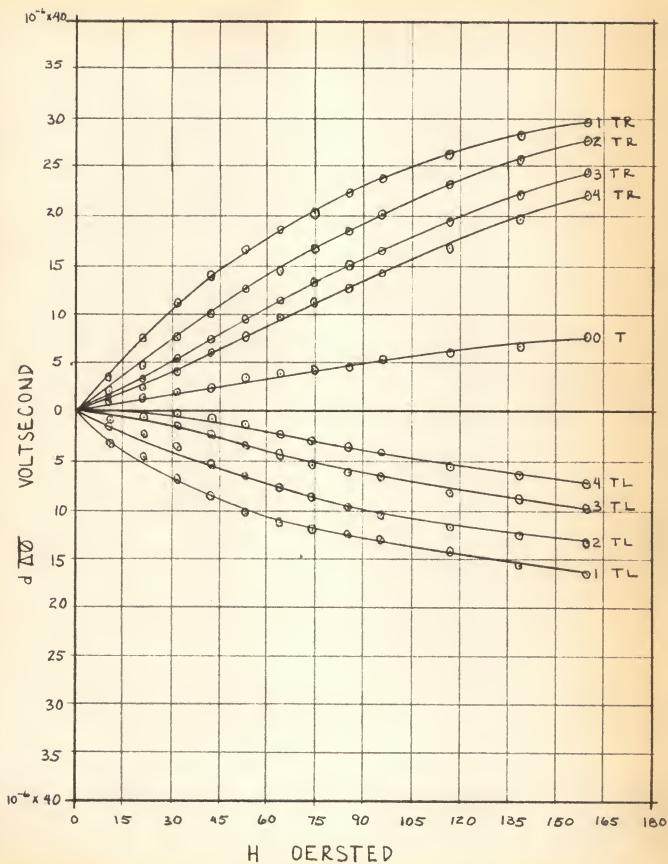
# PLATE VIII

EXPLANATION OF PLATE IX

The experimental magnetization curves for different values of angular displacement (T). One turn equals 3.28 deg/cm. TR designates "turns to right" and TL designates "turns to the left."
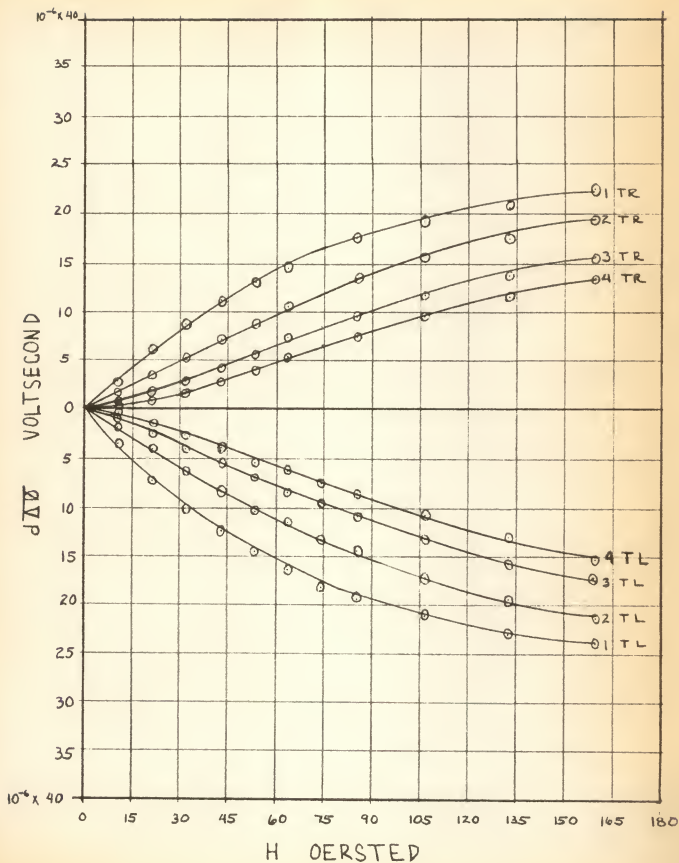
# PLATE IX



$10^{-6} \times 40$

VOLTSECOND

$d\,\Delta \overline{U}$

O1 TR
O2 TR
O3 TR
O4 TR

O 4 TL
O 3 TL
O2 TL
O1 TL

$10^{-6} \times 40$

0  15  30  45  60  75  90  105  120  135  150  165  180

H  OERSTED

EXPLANATION OF PLATE X

The experimental magnetization curves for different values of angular displacement (T). One turn equals 3.28 deg/cm. TR designates "turns to right" and TL designates "turns to the left."
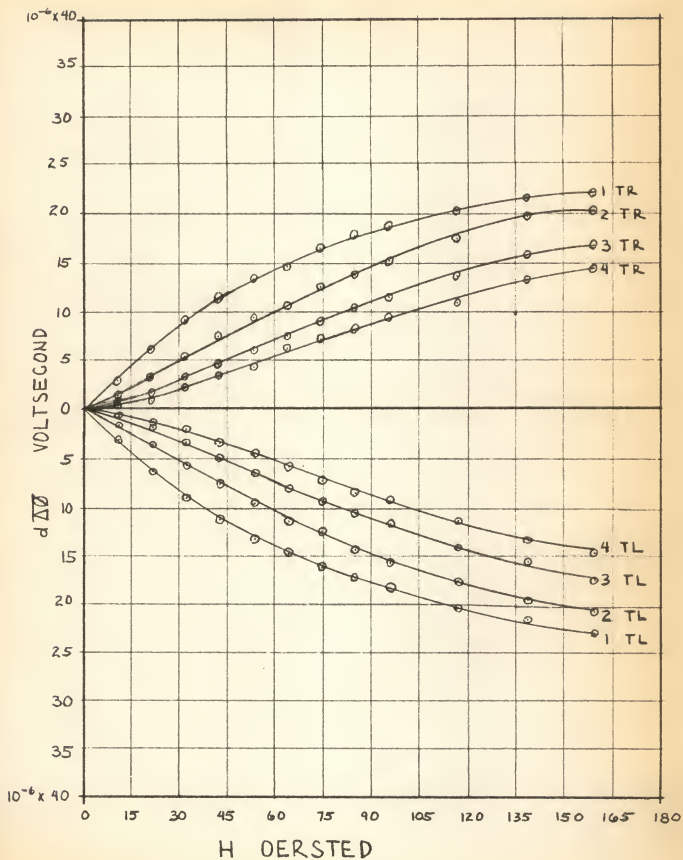
# PLATE X

EXPLANATION OF PLATE XI

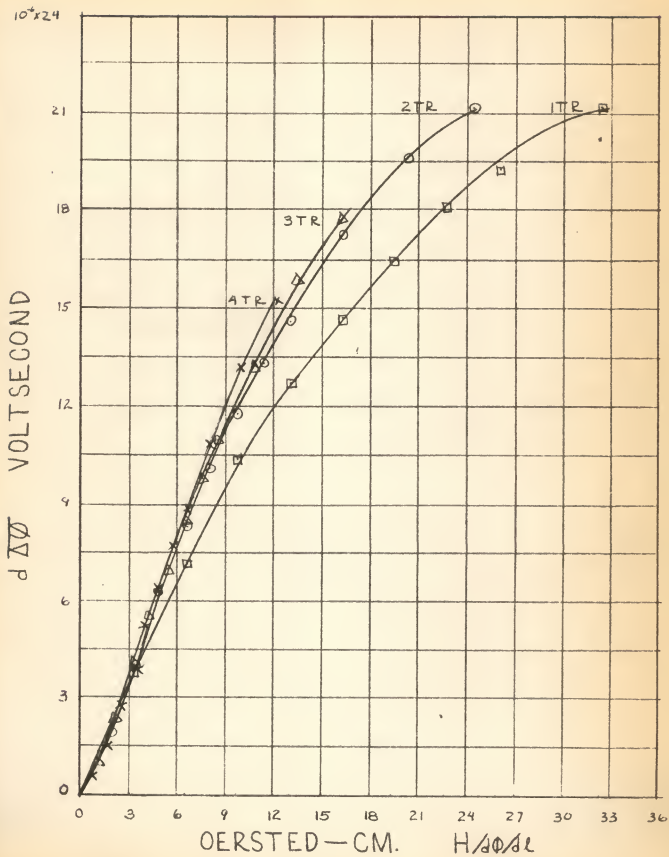Plot of $d\overline{\Delta\phi}$ versus $\dfrac{H}{d\phi/dl}$ for data shown in Plate IX

$\boxdot$ = 1 TR
$\ominus$ = 2 TR
$\triangle$ = 3 TR
$\times$ = 4 TR

# PLATE XI

EXPLANATION OF PLATE XII

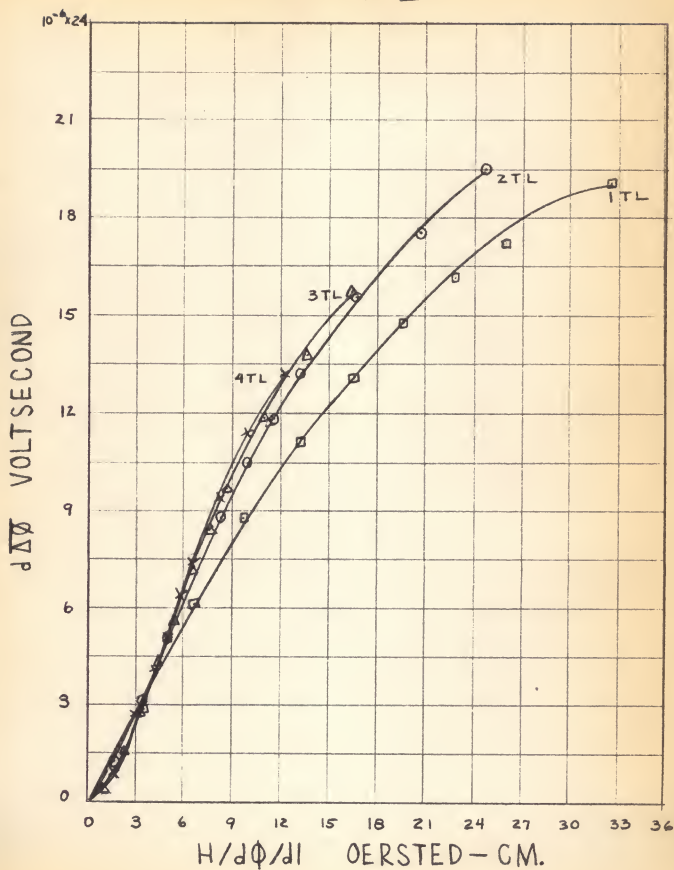Plot of $\overline{d\Delta\phi}$ versus $\dfrac{H}{d\phi/dl}$ for data shown in Plate IX.

⊡ - 1 TL
☉ - 2 TL
△ - 3 TL
✗ - 4 TL

# PLATE XII

## CONCLUSIONS

The simple theoretical model developed by G. J. van der Maas appears to hold promise of describing the reversible quasistatic magnetization processes in ferromagnetic wires. The model is not unreasonable even though internal stress and texture of the samples were neglected. Further investigations of both the longitudinal and circular components of magnetization for other materials would more severely test the adequacy of this model. In future investigations of the circular component of magnetization more attention should be given to the polarization of the samples.

LITERATURE CITED

1. Akulov, N.S.Z.
   Atomic theory of ferromagnetism. Z. Physik. 54:582-7. 1929.

2. Becker, R. and W. Doering.
   Ferromagnetismus. Berlin: J. Springer, 1939.

3. Bitter, F.
   On inhomogeneities in the magnetization of ferromagnetic materials.
   Phys. Rev. 38:1903-05. 1931.

4. Bornemeier, D. D.
   Determination of the longitudinal magnetization curves of polarized nickel
   iron wires under torsional stress. Master's Thesis, Kansas State University.
   1960.

5. Bozorth, R. M.
   Ferromagnetism. New York: D. Van Nostrand, 1951.

6. Dijkstra, L. J. and J. L. Snoek.
   Propagation of large Barkhausen discontinuities in Ni-Fe alloys. Phillips
   Res. Rep. 4:334. 1949.

7. Joule, J. P.
   On the effects of magnetism on the dimensions of iron and steel bars.
   Philosophical Magazine. 30:76-87, 225-241. 1847.

8. Landau, L. and E. Lifshitz.
   Theory of dispersion of magnetic permeability in ferromagnetic bodies.
   Physik Z. Sowjetunion. 8. 1935.

9. Sixtus, K. L. and L. Tonks.
   Propagation of large Barkhausen discontinuities. Phys. Rev. 37:930-58.
   1931.

10. Stewart, K. H.
    Experiment on a specimen with large domain. J. Phys., Radium. 12:325.
    1951.

11. van der Maas, G. J.
    Quarterly progress reports, National Research Council, Canada. 1949, et
    seq.

12. van der Maas, G. J.
    Private communication, 1959.

13. Weiss, P.
    Hypothesis of the molecular field and ferromagnetic properties. J. Phys.
    4:6, 661-90. 1907.

14. Williams, H. J., R. M. Bozorth and W. Schockley.
    Magnetic domains in single crystals of silicon iron. Phys. Rev. 75: 155-
    78. 1949.

APPENDIX

## Stress Analysis of Wire

Since the magnetostrictive strain energy is most simply expressed in terms of the directions of principal stress at any point in the wire, it is expedient to examine the mechanical stress conditions in a twisted rod. In this computation a wire under pure torsion will be examined.

Consider the symmetric stress tensor

$$S = \begin{vmatrix} X_x & Y_x & Z_x \\ X_y & Y_y & Z_y \\ X_z & Y_z & Z_z \end{vmatrix}$$

where $I_j$ represents the force in the I direction on a surface whose normal is in the j direction and

$$X_y = Y_x$$
$$X_z = Z_x$$
$$Y_z = Z_y$$

The stress related to the normal direction $\underline{n}$ of an imaginary cut in the stressed material is given by

$$X_n = X_x \cos a + X_y \cos b + X_z \cos c$$
$$Y_n = Y_x \cos a + Y_y \cos b + Y_z \cos c \qquad (1)$$
$$Z_n = Z_x \cos a + Z_y \cos b + Z_z \cos c$$

where cos a, cos b and cos c are direction cosines. The principal directions of stress for this tensor are found using the condition that the direction of the surface normal $\underline{n}$ and the corresponding force per unit area must be the same. This condition is equivalent to determining the direction a, b, and c for which

$$S \begin{vmatrix} \cos a \\ \cos b \\ \cos c \end{vmatrix} = \lambda \begin{vmatrix} \cos a \\ \cos b \\ \cos c \end{vmatrix} \qquad (2)$$

where $\lambda$ is a scaler. Expanding and rewriting gives

$$(X_x - \lambda) \cos a + Y_x \cos b + Z_x \cos c = 0$$

$$X_y \cos a + (Y_y - \lambda) \cos b + Z_y \cos c = 0 \qquad (3)$$

$$X_z \cos a + Y_z \cos b + (Z_z - \lambda) \cos c = 0$$

Solutions to equation (3) will be non-trivial only if

$$\begin{pmatrix} X_x - \lambda & Y_x & Z_x \\ X_y & Y_y - \lambda & Z_y \\ X_z & Y_z & Z_z - \lambda \end{pmatrix} = 0 \qquad (4)$$

For a small circular disk of the wire with the axis of this disk along Z, the tensor elements are

$$X_z = Z_x = - G \frac{d\phi}{dl} y$$

$$Y_z = Z_y = G \frac{d\phi}{dl} x \qquad (5)$$

$$X_x = Y_y = Z_z = X_y = Y_x = 0$$

where G is the isothermal shear modulus and $\frac{d\phi}{dl}$ is the twist per unit length of the wire. Substitution of the relations in equation (5) into equation (4) and solving for $\lambda$ gives

$$\lambda_1 = G \frac{d\phi}{dl} \rho$$

$$\lambda_2 = - G \frac{d\phi}{dl} \rho$$

$$\lambda_3 = 0$$

where $= (x^2 + y^2)^{\frac{1}{2}}$. Since $\lambda_3 = 0$, there are only two nondegenerate principal direction of stress. Substitution of $\lambda_1$ into equation (3) using equation (5) gives

and

$$\frac{\cos a_1}{\cos c_1} = - \frac{y}{\rho}$$

$$\frac{\cos b_1}{\cos c_1} = \frac{x}{\rho} \qquad (6a)$$

Substitution of $\lambda_2$ into equation (3) using equation (5) gives

$$\frac{\cos a_2}{\cos c_2} = - \frac{y}{\rho}$$

$$\frac{\cos b_2}{\cos c_2} = \frac{x}{\rho} \qquad (6b)$$

Using the relation

$$\cos^2 a + \cos^2 b + \cos^2 c = 1$$

one obtains from equations (6a) and (6b)

$$\cos c_1 = \pm \frac{\sqrt{2}}{2}$$

$$\cos c_2 = \pm \frac{\sqrt{2}}{2}$$

Setting $\cos c_1 = + \sqrt{2}/2$ and $\cos c_2 = - \sqrt{2}/2$ yields from equations (6a) and (6b)

$$\cos a_1 = -\frac{y}{\sqrt{2}\rho} \; ; \quad \cos b_1 = \frac{x}{\sqrt{2}\rho} \; ; \quad \cos c_1 = \frac{\sqrt{2}}{2} \; ; \; c_1 = \pi/4 \tag{7}$$

$$\cos a_2 = -\frac{y}{\sqrt{2}\rho}; \quad \cos b_2 = \frac{x}{\sqrt{2}\rho} \; ; \quad \cos c_2 = -\frac{\sqrt{2}}{2} \; ; \; c_2 = \pi/4$$

This computation gives two vectors

$$\underline{n}_1 = \hat{i} \left(\frac{-y}{\sqrt{2}\rho}\right) + \hat{j} \left(\frac{x}{\sqrt{2}\rho}\right) + \hat{k} \frac{\sqrt{2}}{2}$$

$$\underline{n}_2 = \hat{i} \left(\frac{-y}{\sqrt{2}\rho}\right) + \hat{j} \left(\frac{x}{\sqrt{2}\rho}\right) - \hat{k} \frac{\sqrt{2}}{2}$$

which are orthogonal and perpendicular upon the cylindrical radius vector $\rho$.
The principal stresses are

$$X_1 = - G \frac{d\phi}{dl} \frac{y}{\sqrt{2}}$$

$$Y_1 = + G \frac{d\phi}{dl} \frac{x}{\sqrt{2}}$$

$$Z_1 = + G \frac{d\phi}{dl} \rho/\sqrt{2}$$

$$X_2 = + G \frac{d\phi}{dl} \frac{y}{\sqrt{2}}$$

$$Y_2 = - G \frac{d\phi}{dl} x/\sqrt{2}$$

$$Z_2 = + G \frac{d\phi}{dl} \frac{\rho}{\sqrt{2}}$$

Thus it is seen that there exist two directions of principal stress

$$\sigma_1 = \sigma_+ = \sqrt{X_1^2 + Y_1^2 + Z_1^2} = G \frac{d\phi}{dl} \rho \tag{8}$$

$$\sigma_1 = \sigma_- = \sqrt{X_2^2 + Y_2^2 + Z_2^2} = G \frac{d\phi}{dl} \rho \tag{9}$$

where $\sigma_+$ represents the tensile stress and $\sigma_-$ represents the compressive stress.

Hence this calculation leads to the configuration of the stresses as shown in Figure 1.
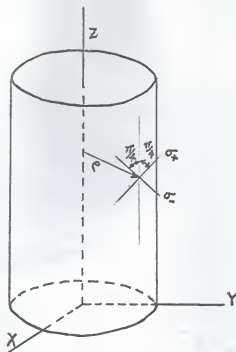
Figure 1

It is seen from equation (7) that a change in the amount of applied twist (dφ/dl) does not change the direction of the principal stresses. The direction of principal stress in the wire is always perpendicular upon the radius vector and makes an angle of 45° with the axis of the wire. It can be shown (12) that the application of a longitudinal stress serves only to reduce the angle between the direction of principal stress and the axis of the wire.

### Determination of $\bar{E}$

In order to prove that $\bar{E}$ has the form

$$E = \frac{1}{\pi r^2} \int_0^r E(\rho) \, 2\pi \rho \, d\rho \tag{1}$$

consider a thin cylinder of the wire radius $\rho$, thickness $\Delta \rho$ and length 1. The resistance $\Delta R$ of this cylinder is

$$\Delta R = \frac{\epsilon l}{2\pi \rho \Delta \rho} \tag{2}$$

where $\epsilon$ is the resistivity of the wire.

The emf generated in the cylinder may be related to the electric field in the cylinder through the relation

$$emf = - E(\rho) \, l \tag{3}$$

Let the cylinder be approximated by a battery with an emf as given by equation
(3) in series with a resistance given by equation (2) through which a current
i flows. The voltage drop across the ends of the cylinder is then

$$V = - E(\rho) - i(\rho) \ \Delta R(\rho)$$

or

(4)

$$V = - E(\rho) - 2 \pi j(\rho) \rho \ \Delta \rho \ \Delta R(\rho)$$

where $j(\rho)$ is the current density in the cylinder. Substitution of equation
(2) into equation (4) gives

$$V = - E(\rho)\ell - j(\rho)\varepsilon\ell$$

(5)

Let the wire be approximated by a large number N of elemental cylinders
where each cylinder has a different emf, a different resistance and different
current.[1] That is, the wire is approximated by N series circuit elements con-
nected in parallel. It is easily shown that there exists only current flow
parallel to the axis of the wire.

Since there is negligible current flow in the circuit external to the wire,

$$\sum_{K=1}^{N} i_{k} = 0$$

Where $N = r/\Delta\rho$ and r is the radius of the wire. In terms of the current densi-
ty

$$2\pi \sum_{K=1}^{N} j_{k} \rho_{k} \ \Delta \rho_{k} = 0$$

If N is then allowed to become infinitely large, the above relation becomes

$$\int_{0}^{r} j(\rho) \ \rho \ d\rho = 0$$

(6)

Integration of equation (5) from 0 to r over $\rho \, d\rho$ yields

$$\int_{0}^{r} V \rho \, d\rho = - \ell \int_{0}^{r} E(\rho) \rho \, d\rho - \varepsilon \ell \int_{0}^{r} j(\rho) \rho \, d\rho$$

Using equation (6) in the above relation and integrating gives

$$V = - \frac{2\ell}{r^2} \int_{0}^{r} E(\rho) \rho \, d\rho$$

or

(7)

$$V = - \frac{\ell}{\pi r^2} \int_{0}^{r} E(\rho) \ 2\pi\rho \, d\rho$$

---

[1] A calculation of the maximum value of the energy dissapted by the wire
due to eddy currents was found to be less than $2 \times 10^{-4}$ watts per meter of wire.

It is also noted that in general

$$V = -\bar{E}\ell \qquad (8)$$

Comparing equations (7) and (8) it is seen that

$$\bar{E} = \frac{1}{\pi r^2} \int_0^r E(\rho)\, 2\pi \rho\, d\rho$$

Hence that form of $\bar{E}$ has been proven.

## Integration of Equation (28a)

Rewriting equation (28a)

$$\Delta \ell(\rho) = A \int_{\theta_\rho}^{\theta_r} \sin\theta\, d\left(\frac{\sin\theta}{\cos 2\theta}\right)$$

where

$$A = \frac{\ell I_s^2 H}{3 \lambda_s G \frac{d\phi}{d\ell}}$$

Integration by parts yields

$$\Delta \ell(\rho) = A \left[ \frac{\sin^2\theta}{\cos 2\theta} \Big|_{\theta_\rho}^{\theta_r} - \int_{\theta_\rho}^{\theta_r} \frac{\sin\theta}{\cos 2\theta}\, d(\sin\theta) \right]$$

Noting that $\ell n |\cos 2\theta| = \ell n |1 - \sin^2\theta|$

and

$$d\left(\ell n |\cos 2\theta|\right) = -4 \frac{\sin\theta}{\cos 2\theta}\, d(\sin\theta)$$

the above relation integrates to

$$\Delta \ell(\rho) = \frac{\ell I_s^2 H}{3\lambda_s G \frac{d\phi}{d\ell}} \left[ \frac{\sin^2\theta}{\cos 2\theta} + \frac{1}{4} \ell n |\cos 2\theta| \right]_{\theta_\rho}^{\theta_r}$$

which is equation (28b).

## Integration of Equation (29a)

Rewriting equation (29a)

$$\overline{\Delta \ell} = \frac{\ell I_s B^3}{r^2} \int_0^{\theta_r} \left[ \frac{\sin^2\theta}{\cos 2\theta} + \frac{1}{4} \ell n |\cos 2\theta| \right]_{\theta_\rho}^{\theta_r} d\left( \frac{\sin^2\theta_\rho}{\cos^2 2\theta_\rho} \right)$$

where

$$B = \frac{I_s H}{3 \lambda_s G} \frac{d\phi}{d\ell}$$

Integration by parts yields

$$\overline{\Delta\emptyset} \;=\; \frac{\ell\, I_s\, B^3}{r^2} \left\{ \left[ \frac{\sin^2\theta}{\cos 2\theta} + \frac{1}{4}\, \ell n\, |\cos 2\theta| \right]_{\theta_\rho}^{\theta_r} \left[ \frac{\sin^2\theta_\rho}{\cos^2 2\theta_\rho} \right] \right|_{\theta_\rho = 0}^{\theta_\rho \,=\, \theta_r}$$

$$- \int_0^{\theta_r} \frac{\sin^2\theta_\rho}{\cos^2 2\theta_\rho} \; d\left[ \left( \frac{\sin^2\theta}{\cos 2\theta} + \frac{1}{4}\, \ell n\, |\cos 2\theta| \right)_{\theta_\rho}^{\theta_r} \right] \right\}$$

$$=\; \frac{\ell\, I_s\, B^3}{r^2} \left\{ \left[ \frac{\sin^2\theta_r}{\cos 2\theta_r} + \frac{1}{4}\, \ell n\, |\cos 2\theta_r| - \frac{\sin^2\theta_\rho}{\cos 2\theta_\rho} - \frac{1}{4}\, \ell n\, |\cos 2\theta_\rho| \right] \right.$$

$$\left. \left[ \frac{\sin^2\theta_\rho}{\cos^2 2\theta_\rho} \right] \right|_{\theta_\rho = 0}^{\theta_\rho \,=\, \theta_r} - \int_0^{\theta_r} \frac{\sin^2\theta_\rho}{\cos^2 2\theta_\rho} \; d\left[ \left( \frac{\sin^2\theta}{\cos 2\theta} + \frac{1}{4}\, \ell n\, |\cos 2\theta| \right)_{\theta_\rho}^{\theta_r} \right] \right\}$$

$$=\; \frac{\ell\, I_s\, B^3}{r^2} \int_0^{\theta_r} \frac{\sin^2\theta_\rho}{\cos^2 2\theta_\rho} \; d\left[ \left( \frac{\sin^2\theta}{\cos 2\theta} + \frac{1}{4}\, \ell n\, |\cos 2\theta| \right)_{\theta_\rho}^{\theta_r} \right]$$

But

$$d\left[ \left( \frac{\sin^2\theta}{\cos 2\theta} + \frac{1}{4}\, \ell n\, |\cos 2\theta| \right)_{\theta_\rho}^{\theta_r} \right]$$

$$=\; d\left( \frac{\sin^2\theta_\rho}{\cos 2\theta_\rho} \right) + \frac{1}{4}\, d\left( \ell n\, |\cos 2\theta_\rho| \right) + d\left( const. \right)$$

Which gives

$$\overline{\Delta\emptyset} \;=\; \frac{\ell\, I_s\, B^3}{r^2} \left( I_1 + I_2 \right)$$

Where

$$I_1 = \int_0^{\theta_r} \frac{\sin^2 \theta_e}{\cos^2 2\theta_e} \, d\left(\frac{\sin^2 \theta_e}{\cos 2\theta_e}\right)$$

and

$$I_2 = \int_0^{\theta_r} \frac{\sin^2 \theta_e}{\cos^2 2\theta_e} \, d\left(\ln|\cos 2\theta_e|\right)$$

Consider $I_1$ dropping the subscript. First it is noted that

$$\cos 2\theta = 1 - 2\sin^2 \theta$$

So

$$d\left(\frac{\sin^2 \theta}{\cos 2\theta}\right) = d\left(\frac{1}{2\cos 2\theta}\right)$$

Substituting the above relations into $I_1$ gives

$$I_1 = \frac{1}{4} \int_{\theta=0}^{\theta=\theta_r} \frac{1}{\cos^2 2\theta} \, d\left(\frac{1}{\cos 2\theta}\right) - \frac{1}{4} \int_{\theta=0}^{\theta=\theta_r} \frac{1}{\cos 2\theta} \, d\left(\frac{1}{\cos 2\theta}\right)$$

Letting

$$X = \frac{1}{\cos 2\theta} \qquad ; \qquad dX = d\left(\frac{1}{\cos 2\theta}\right)$$

The above relation becomes

$$I_1 = \frac{1}{4} \int_{\theta=0}^{\theta=\theta_r} X^2 dX - \frac{1}{4} \int_{\theta=0}^{\theta=\theta_r} X \, dX$$

Integration yields

$$I_1 = \left[\frac{1}{12\cos^3 2\theta} - \frac{1}{8\cos^2 2\theta}\right]_0^{\theta_r}$$

Consider $I_2$

$$I_2 = \frac{1}{4} \int_{\theta=0}^{\theta=\theta_r} \frac{\sin^2 \theta}{\cos^2 2\theta} \, d\left(\ln|\cos 2\theta|\right)$$

$$I_2 = \frac{1}{8} \int_{\theta=0}^{\theta=\theta_r} \frac{(1-\cos 2\theta)}{\cos^3 2\theta} \, d(\cos 2\theta)$$

Letting

$$y = \cos 2\theta \quad ; \quad dy = d(\cos 2\theta)$$

$$I_2 = -\frac{1}{8} \int_{\theta=0}^{\theta=\theta_r} x^{-2} \, dx + \frac{1}{8} \int_{\theta=0}^{\theta=\theta_r} x^{-3} \, dx$$

$$= \left[ \frac{1}{8\cos 2\theta} - \frac{1}{16\cos^2 2\theta} \right]_0^{\theta_r}$$

Hence

$$\overline{\Delta\phi} = \frac{\ell I_s B^3}{r^2} \left[ \frac{1}{12\cos^3 2\theta} - \frac{3}{16\cos^2 2\theta} + \frac{1}{8\cos 2\theta} \right]_0^{\theta_r}$$

or

$$\overline{\Delta\phi} = \frac{\ell I_s B^3}{r^2 \cos^3 2\theta_r} \left[ \frac{1}{12} - \frac{3}{16}\cos 2\theta_r + \frac{1}{8}\cos^2 2\theta_r - \frac{1}{48}\cos^3 2\theta_r \right]$$

From equation (25) page 13 one sees

$$\cos^3 2\theta = \frac{B^3}{\rho^3}\sin^3\theta$$

or

$$\cos^3 2\theta_r = \frac{B^3}{r^3}\sin^3\theta_r$$

Hence

$$\overline{\Delta\phi} = \frac{\ell I_s r}{\sin^3\theta_r} \left| \frac{1}{12} - \frac{3}{16}\cos 2\theta_r + \frac{1}{8}\cos^2 2\theta_r - \frac{1}{48}\cos^3 2\theta_r \right]$$

INVESTIGATION OF THE CIRCULAR MAGNETIZATION
CURVE FOR NICKEL-IRON WIRES UNDER
TORSIONAL AND TENSILE STRESS

by

ARLYN EUGENE ASCH

B. S., Midland College, 1957

———

AN ABSTRACT
OF A MASTER'S THESIS

submitted in partial fulfillment of the

requirements for the degree

MASTER OF SCIENCE

Department of Physics

KANSAS STATE UNIVERSITY
Manhattan, Kansas

1962

A theory derived by G. J. van der Maas for the behavior of the circular component of magnetization of a twisted ferromagnetic wire in a longitudinal magnetic field is presented in detail. The theoretical results are expressed in terms of two parametric equations relating the externally applied longitudinal magnetic field and the total change in flux in the wire. The change in flux is exhibited by a voltage pulse developed across the ends of the wire. Theoretical considerations also indicate that the change in the circular component of magnetization is a function of the magnetic field intensity divided by the applied twist. These results were derived under the assumption that the total free energy is given by the sum of the magnetoelastic and field energies.

The purpose of this research was an attempt to verify experimentally the theoretical model derived by G. J. van der Maas.

The wire samples (51 percent nickel - 49 percent iron) were magnetically annealed by heating them above their curie point ($510^{\circ}$C) and allowing them to cool rapidly in a longitudinal magnetic field while subjected to tensile stress. The samples were then placed in a longitudinal rectified DC magnetic field, and the change in the circular component of magnetization of the wire was measured as a function of the applied field and the angular displacement of the wire.

The experimental results, while 25 to 30 percent below the theoretically predicted results, indicate that the simple model holds promise of describing stressed ferromagnetic wires even though internal stress and texture of the wire were neglected. It was also found that the change in the circular component of magnetization was very nearly a function of the applied field divided by the twist, provided the twist was greater than 5 deg/cm.